TECHNICAL REVIEW

No.23 / March 2025

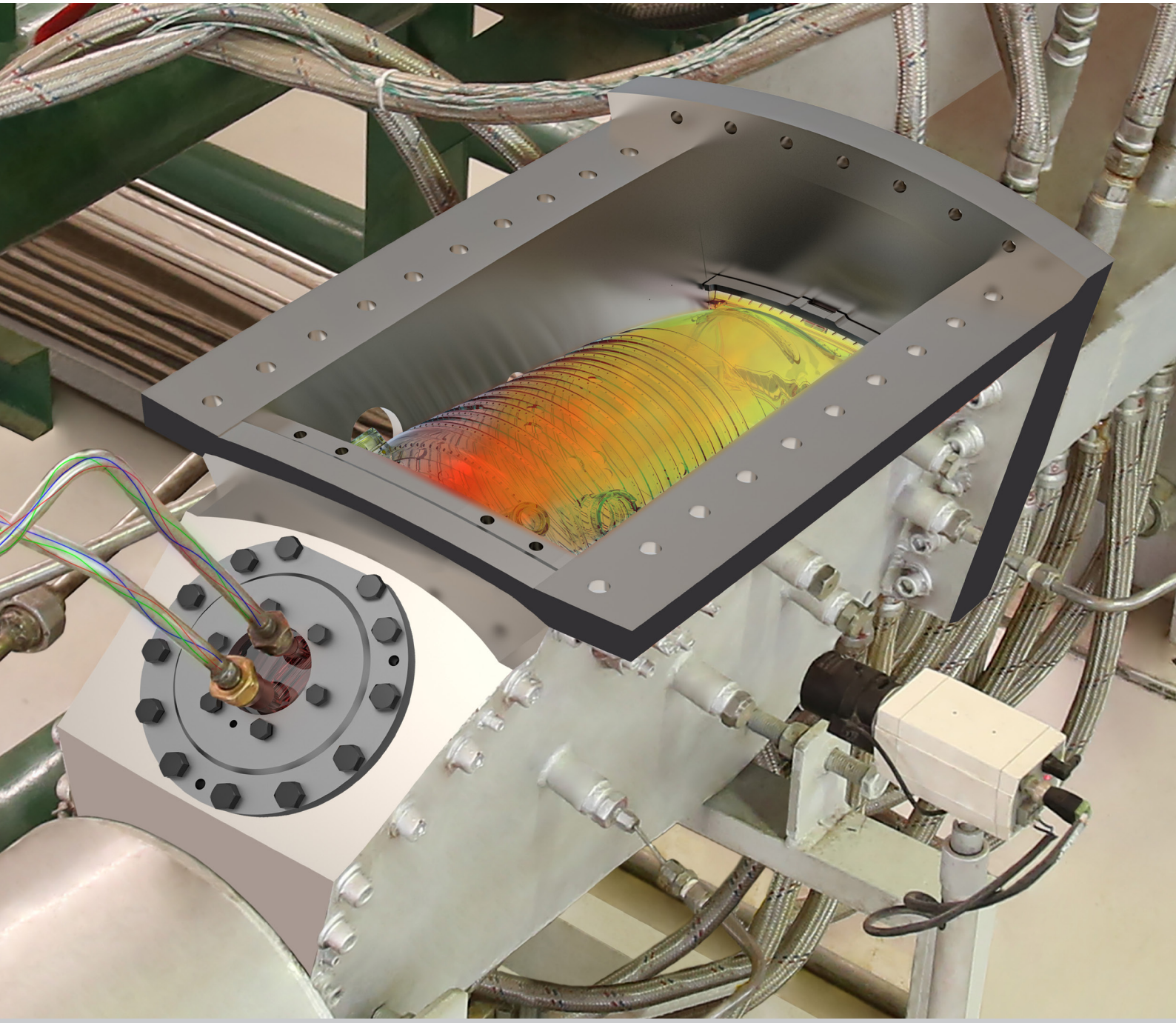

Technical Review

MAPNA TURBINE ENGINEERING & MANUFACTURING CO. (TUGA)

TUGA

MAPNA GROUP

Willpower to Empower Generations

TECHNICAL REVIEW

Editorial & Production

Cover Page:
TUGA's Hydrogen Combustion Test Bench

Editorial

Dear Colleagues, Partners and Professionals,

At MAPNA Turbine (TUGA), we are dedicated to proficiently developing, manufacturing, and delivering comprehensive services for gas turbines, steam turbines, and compressors essential to the energy industries across both domestic and international markets. It is in this context, and with great pleasure, that we present to you, our valued readers, a brief account of a few recent technological achievements in this edition of TUGA Technical Review.

In line with global sustainability trends, MAPNA is dedicated to developing clean energy technologies related to hydrogen fuel. The first article reviews recent improvements to TUGA's hydrogen combustion test and prototype manufacturing infrastructure and provides an account of the hydrogen combustion tests for the advanced DLE burner of the MGT-30 industrial gas turbine.

The second article introduces TUGA's new test facility for hydrostatic, helium, and gas leak tests. This test bench helps TUGA gain market share and solidify its reputation as a leading company in the compressor industry by ensuring that the centrifugal compressors designed and manufactured by the company comply with international standards and meet customer needs.

The third article outlines the main features and modules of TUGA's native performance software, MapCycle. This software provides an accurate and up-to-date physical model of gas turbines integrated with auxiliary systems and components. The MapCycle workflow is designed to cover concepts like performance digital twin and condition monitoring, as well as big data technologies, online services for project engineering, and interface with TAPP as TUGA CRM.

The fourth article elaborates on the importance of addressing surface roughness of additively manufactured parts to obtain high-quality components. It investigates sandblasting (SB) and vibratory surface finish (VSF) as two readily available, effective, and cost-efficient processes that can be used for surface quality improvements.

In an attempt to investigate the possibility of eliminating PWHT to reduce repair time, equipment outage time, and the cost of welding operations, the final article studies and compares the effects of welding with nickel-based filler, TBW, and welding with PWHT on the mechanical properties of samples.

Please join us in exploring a detailed account of these subjects in this issue of the Technical Review.

Respectfully,

Roohollah Jabery,

Vice President for Engineering and R&D

MAPNA Turbine Company (TUGA)

March 2025

Contents

1

Hydrogen Combustion Test, a Great Step toward Sustainable Future

Shaye, Ali
Esmailli, Milad
Ranjbaran, Alireza

MAPNA Turbine Engineering & Manufacturing Co. (TUGA)

Introduction

Global warming, driven by greenhouse gases like carbon dioxide and methane, poses a risk to the ecosystems that we all rely on. According to the Paris Agreement, an international commitment on climate change was required, strengthening efforts and policies worldwide for the transition to a low-carbon energy system. Many countries have made commitments to reducing economy-wide greenhouse gas emission by more than 50% by 2030, compared to 1990 levels and achieving net-zero emission by 2050. Gas turbines play an important role in the energy transition and enabling the future net-zero energy system, while major reduction in carbon emission can be achieved by adding hydrogen to the natural gas fuel with ultimate zero carbon emission when pure hydrogen is used. Additionally, by operating with hydrogen fuel, gas turbines provide more grid stability and support for intermittent renewable energy sources such as wind and solar.

In line with global approaches and other OEMs, MAPNA is dedicated to developing clean energy technologies related to hydrogen fuel. In this regard, MAPNA Turbine (TUGA) has planned a comprehensive technological roadmap for combustion system design and has expanded the R&D activities by improving the infrastructures of test and prototype manufacturing.

Combustion Laboratory Retrofit

Hydrogen combustion is a new field of research and development in the gas turbine industry. Generally, and regardless of advancements in design methods, experimental tests still play a great role in the development process of combustion systems. As a result, TUGA's atmospheric combustion test stand has been developed to characterize several aspects of combustion explained in detail in TR NO. 6. The existing combustion test stand is planned to have the additional capability for hydrogen-natural gas mixing and testing the hydrogen fueled gas turbine burners.

Figure 1 - TUGA's atmospheric combustion test stand

There are several operational challenges with hydrogen relating to safety issues. Hydrogen can diffuse through seals that might be considered airtight or impermeable to other gases. Therefore, traditional sealing systems used with natural gas may need to be replaced with welded joints or other appropriate components. Additionally, hydrogen is colorless, odorless and more flammable than methane. Therefore, any leakage could increase safety risks requiring changes to plant procedures.

Considering the above-mentioned issues, precise safety evaluation and risk analysis of the mixing skid are mandatory. This evaluation consists of different aspects, including HAZOP/HAZID study, Fire Safety Design (FSD) and also Hazardous Area Classification (HAC).

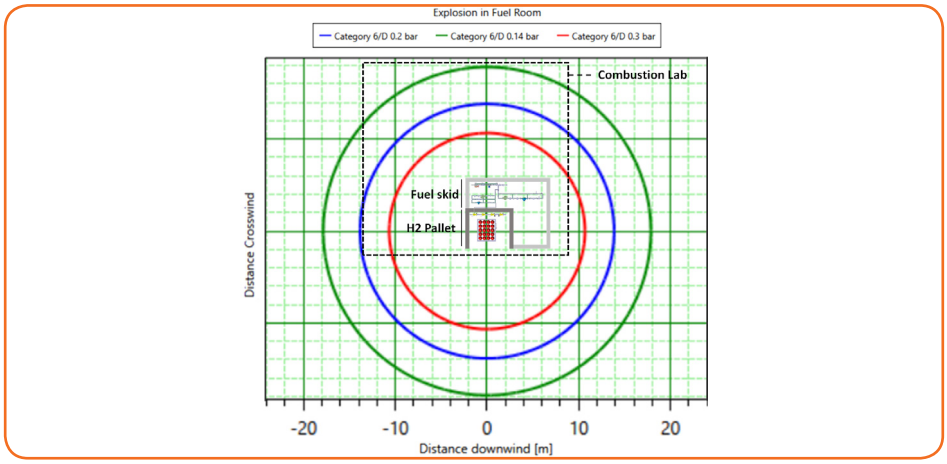

Figure 2 - Explosion pressure contour for worst case scenario of consequence modelling

According to this evaluation, the hydrogen-NG fuel mixing skid should be located in a separate fuel room outside the laboratory. In this room, a specific place is designated for the hydrogen cylinder pallet surrounded by reinforced concrete walls to protect fuel room equipment from potential explosions. Also, a firewall is placed in front of the open side of the cylinder room.

An isolated earthing system is established for the fuel mixing room that connects all equipment and structures to the ground, protecting them from possible electrostatic sparks in the hydrogen-containing zone.

Fuel Mixing Skid Design

In order to mix hydrogen with natural gas for testing the burners in the atmospheric test bench, it is necessary to design a new fuel skid. This skid must be designed and manufactured in accordance with the safety requirements for hydrogen use and with sufficient accuracy to mix different percentages of hydrogen and natural gas. Depending on atmospheric test stand specifications and test plan requirements for the combustion systems, the fuel skid design parameters are considered as shown in the table below.

Table 1 - Design parameters of the fuel mixing skid

	Max Pressure (bar)	Max Flowrate (Kg/h)	Thermal Capacity (kW)
Hydrogen	10	10	250
NG	10	50	500

The fuel mixing skid is designed based on process calculations and software simulations. In addition, all equipment is selected according to the proper explosion-proof specifications for hydrogen service. The final skid P&ID is depicted in Figure 3.

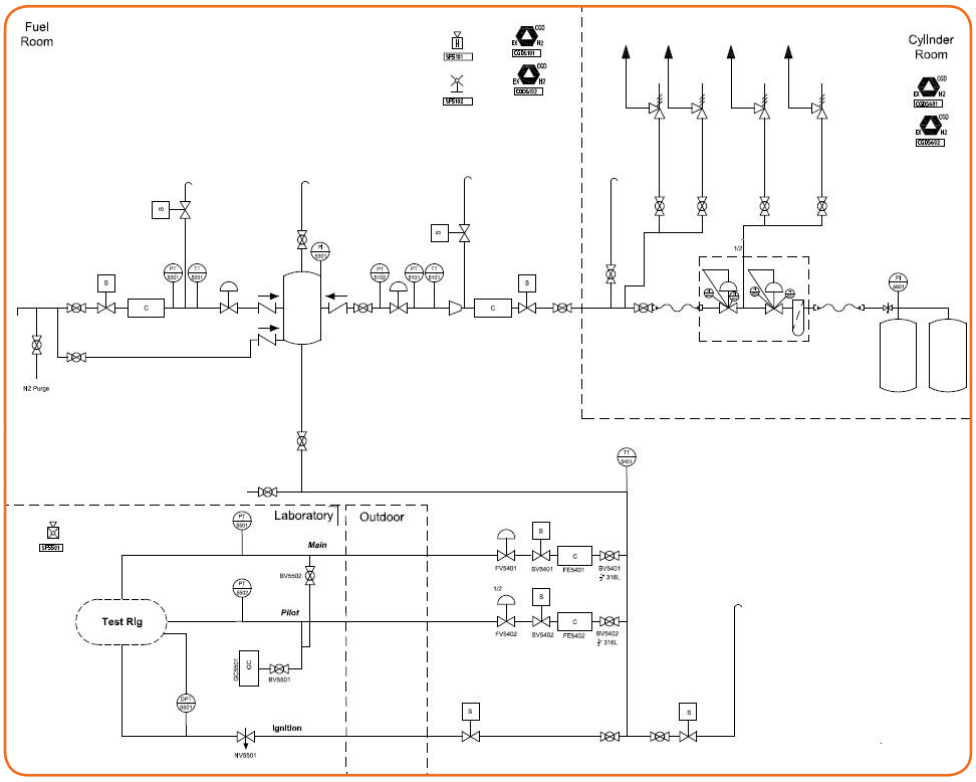

Figure 3 - Fuel mixing skid P&ID

Precise control valves with pneumatic actuators have been used for regulating the flowrate of hydrogen and natural gas, and highly accurate Coriolis flow meters measure and monitor the flow rate passing through the lines. Natural gas enters the designed mixer section and the hydrogen is injected into the natural gas cross flow and the complete mixing of the two gases occurs inside the mixer and the downstream pipes. Afterwards, the fuel gas is delivered in three lines to the test bench in the laboratory. Dedicated control valves and flowmeters in the pilot and main fuel lines are used for metering mixed fuel flowrate from combustion start to any target operational test point. Additionally, a separate line with an on-off valve is used to feed the test rig ignitor.

The hydrogen required for the combustion tests is stored in high-pressure cylinders and located in a pallet for easy transportation. The pallet is placed in the cylinder room and connected to the two-stage regulating panel. Two Pressure Safety Valves (PSV) are provided for each pressure reduction stage to protect the downstream piping from over-pressurizing.

A 3D model of the mixing skid is shown in Figure 4. The placement of skid equipment, instruments and the piping components are specified in this model.

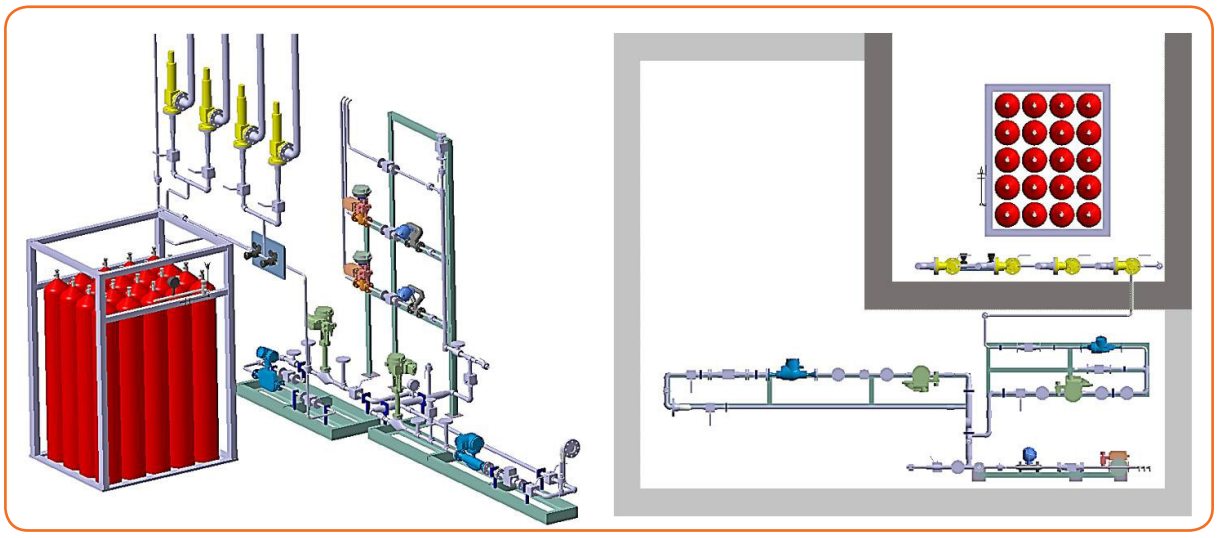

Figure 4 - Fuel mixing skid 3D model

F&G System Design

To detect possible hydrogen leaks, four hydrogen sensors have been considered. Two sensors are installed in the cylinder room on the top of the hydrogen pallet and the other two are installed in the fuel room on top of the mixing skid. The sensors detect the hydrogen amount in the surrounding atmosphere as a percentage of LEL (Lower Explosive Limit). Two points of 5% and 10% LEL have been set for alarm and shutdown signals. Correspondingly, a warning sounder and flasher specifically placed in the laboratory and cylinder room will be activated by the alarm signal.

Control System Modification

In this project, a specific PLC-based control system is developed for the new skid integrated into the previous one. The control system hardware is PLC S7-300, and SIMATIC step7 V5.6 is used for programming. An isolated control module is also designed for the F&G system with its parts located in the control panel. This module has an independent power supply, which is connected to the UPS to increase the safety level. Based on fuel mixing skid configuration, a new HMI has been designed, making it more user-friendly and compatible with requirements and procedures.

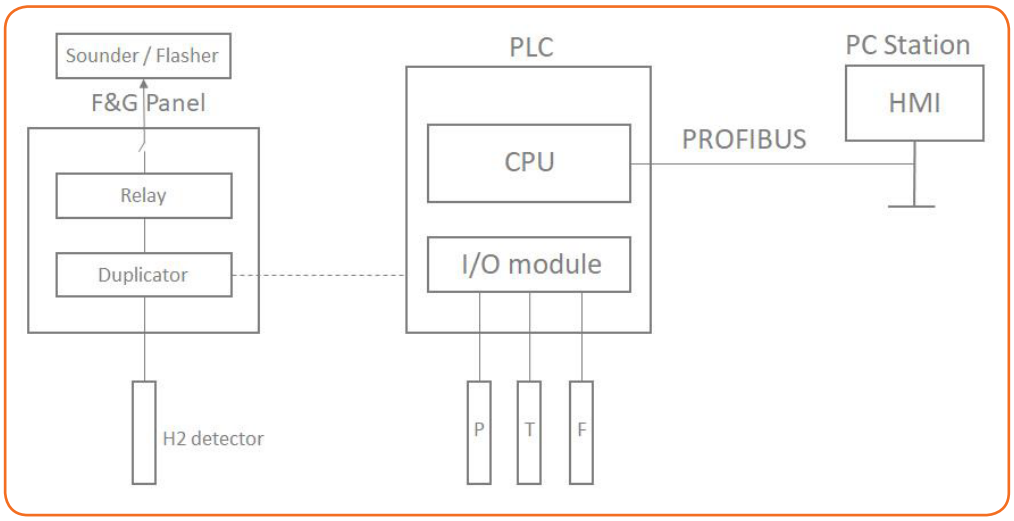

Figure 5 - Control system concept

Fabrication, Installation and Commissioning

The fuel skid piping and equipment installation were carried out according to the design layout in the fuel room. Necessary NDT, such as RT/PT/VT for all welds and pressure tests like hydrostatic and leak tight tests were implemented according to ASME B31.12 for hydrogen service. Afterwards, all skid sections were purged with air and nitrogen to clean up, ensuring that the piping is free of dust, water, and possible contaminants during fabrication, assembly, erection, and testing.

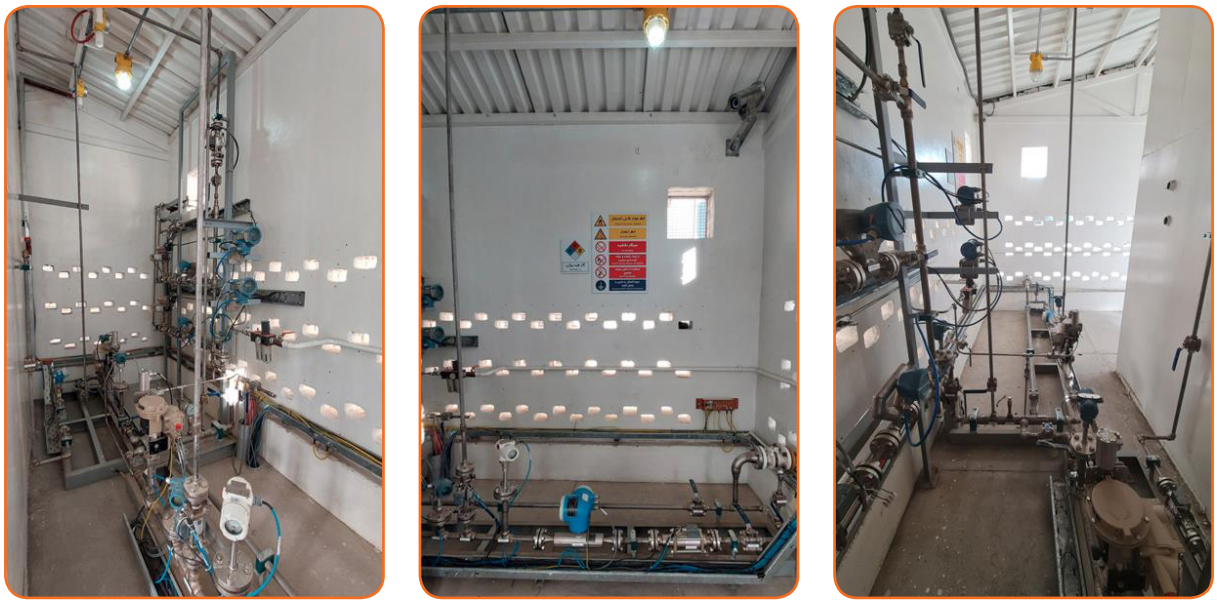

Figure 6 - Fabricated fuel mixing skid

The new fuel system was successfully commissioned initially using compressed air, and the performance of the control valves, flow meters, and other instruments was evaluated. Before conducting hot tests, the fuel skid was purged with nitrogen to ensure the piping is free of oxygen.

Burner Test Rig Preparation

As described in TR No. 11 & TR No. 19, TUGA has developed an advanced DLE burner for the MGT-30 industrial gas turbine, which has been successfully operating in the fleet. Considering the existing test rig infrastructure for this combustion system, it has been planned to run hydrogen combustion tests using this type of premixed burner to determine the hydrogen burning capability of this combustor.

Burning hydrogen-rich fuels inherently increases the risk of flashback due to the higher flame speed and shorter ignition delay time of hydrogen compared to natural gas. Thus, premixed burners using a high percentage of hydrogen, require higher flow velocities in the premixing channels where fuel and air are mixed, to ensure protection against hydrogen flame flashback. In this regard, In addition to the available sensors of DLE combustor test rig, the required additional temperature sensors are installed on the burner to evaluate the thermal behavior of the combustor and prevent the burner from possible flashback phenomena during the hydrogen burning tests. The thermocouples were installed in specified positions to detect flashback and any change in the position of the flame relative to the burner.

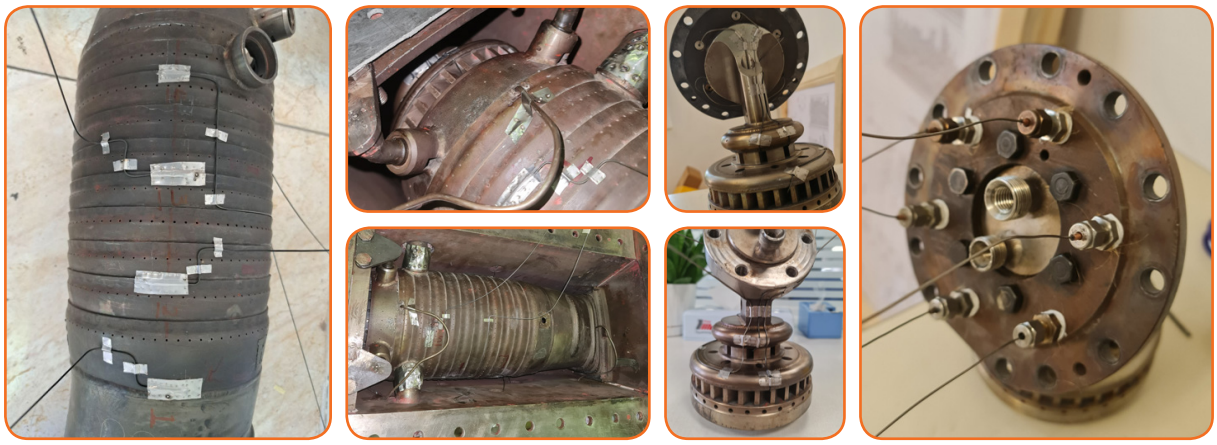

Figure 7 - DLE burner sensoring

In order to assess any deviation in thermal loads on the liner owing to the different characteristics of the hydrogen flame compared to natural gas, temperature sensors are also installed on the liner. The location of the sensors was selected based on thermal loading pattern and temperature spikes on the liner according to the CFD analysis and operational feedback. The obtained test results could then be used to validate combustor numerical simulations.

Tests and Results

Ensuring that all safety and technical requirements were met, the fuel mixing skid was put into operation. At first, the burner was ignited with natural gas, and the condition of the instruments and test stand equipment was checked. After that, according to the test procedure, calculated amounts of hydrogen were gradually fed into the fuel stream. At each point, all important operational parameters such as flame stability, burner and liner temperatures, and combustor exhaust gas temperature profile were checked and recorded besides monitoring the other process parameters and safety signals.

Consequently, the DLE combustor design was approved for burning up to 45% hydrogen with stable flame characteristics and all operational parameters within acceptable range. This amount of hydrogen obviously demonstrates the advanced design technology of this premixed pilot stabilized DLE burner of the MGT-30 industrial gas turbine.

2

Reliability Meets Compliance: Tuga's New Hydrostatic Test Bench for Centrifugal Compressors

ZaeimKohan, Mahdi
Joodaki, Mahdi
KhaliliAbhari, Mani
Abdollahi, Elyas
Rostami, Arash
Lashgari, Reza
Javadi, MohammadAmin

MAPNA Turbine Engineering & Manufacturing Co. (TUGA)

Introduction

In design and manufacture of rotary equipment, compliance with international standards has become a fundamental factor for meeting customer requests, gaining market share and ensuring business survival. In the field of centrifugal compressors, adhering to design, construction, and operational standards is a basic requirement for both customers and employers in the industry. Among the most important processes emphasized by clients in manufacture and assembly of compressors to ensure safe and normal operation are hydrostatic and leak tests.

In line with its mission in compressor design and production, TUGA has decided to create an infrastructure for conducting hydrostatic tests followed by helium and gas leakage tests. A review of some key features of TUGA's test bench are provided in this article.

Test Procedure

The hydrostatic test is a critical procedure used to verify the structural integrity of centrifugal compressors.

After a successful hydrostatic test, and in accordance with the process gas intake and the employer's requirements, helium leak test may be conducted.

The helium leak test is a highly sensitive method used to detect leaks in centrifugal compressors and other critical equipment. This test is essential in ensuring the integrity of the compressor, particularly in applications such as oil and gas industry where gas containment is crucial.

Helium leak test is an effective method for detecting both small and large leaks in larger volumes. Small and light molecules of helium can easily escape through tiny openings, making it an ideal tracer gas for leak detection, where its concentration is measured to identify leaks.

The gas leak test is a method used to assess allowable leakage from dry gas seals after the compressor has been fully assembled. This test is crucial for ensuring safe and efficient operation of the compressor.

TUGA's Test Bench

TUGA's test bench can perform hydrostatic tests on compressor casings at pressures up to 800 bar and gas leak tests at 300 bar. Additionally, it is designed to accommodate various equipment sizes. Based on international standards and our engineering team's best practices, the design and construction of the test bench comply with all safety requirements and follow the standards and guidelines approved by the clients.

As mentioned, the fluids used in the tests include water for the hydrostatic test, helium gas for the helium test (in accordance with the process gas intake and employer's suggestions, optional after a successful hydrostatic test), and nitrogen gas for the leak test, which occurs after complete assembly.

One of the key features of this test station is its ability to handle a wide range of pressure levels and accommodate various casing dimensions for testing. This flexibility presents a significant opportunity for TUGA to generate income by offering testing services to other companies and industrial centers.

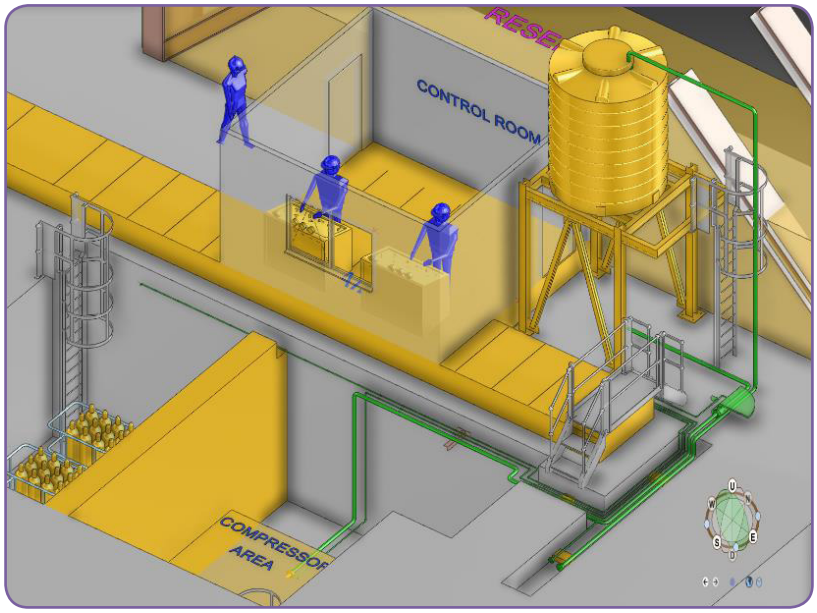

Figure 1 - TUGA's Hydrostatic and gas leak test bench

The new facility has been designed to address specific challenges related to high hydrostatic pressure and gas leakage. Our designs adhere to all relevant standards and safety considerations, utilizing an improved layout that minimizes the space required within the complex. In this context, and based on our high pressure applications, traditional piping systems based on ASME standard cannot be used. After conducting extensive studies, it was decided to implement tubing connections instead.

Using tubing connections that rely on fittings instead of welding improves safety and reduces the space needed. This design enables implementation of pressure generation packages and a tube-drawn path for hydrostatic and gas leakage tests, ensuring a safer and more efficient test process.

Due to the test stand's location within the steam turbine nave, safety measures are top priority. Concrete slabs are strategically placed at the test site to enhance safety during the test process and to provide stability in the event of a failed test. Additionally, multiple cameras are installed to closely monitor the test process.

In accordance with engineering standards, the rate of pressure increase during both hydrostatic and gas leakage tests is capped at 5 bar/min. Furthermore, the evacuation and pressure reduction processes are designed to be smooth and controlled. Consequently, specialized pressure-boosting packages have been developed, and appropriate equipment has been selected to meet these requirements.

Due to the high capacity and critical nature of this test station, several HAZOP meetings were held during the engineering phase to thoroughly assess potential hazards and ensure compliance with safety requirements for its construction and commissioning phase. These meetings took place after the design and engineering documents were finalized, allowing us to identify and mitigate risks effectively. The equipment supply process was proceeded based on these documents, across various sectors including construction, mechanical, instruments, electrical, as well as process and control.

Concluding Remarks

The implementation of hydrostatic and gas leak test bench in TUGA has proven essential in conducting safe and thorough testing in alignment with the API 617 standard, as well as other relevant international standards. TUGA's capability to perform hydrostatic tests at pressures up to 800 bar and gas leak tests at pressures up to 300 bar ensures the integrity and reliability of a diverse range of casing sizes and assembled centrifugal compressors.

This facility not only enhances our testing proficiency but also underscores our commitment to maintaining the highest safety and quality standards in our operations, and solidifying our reputation as a leading company in the compressor industry.

References

[1] ASME VIII, Div 1 Edition 2023

[2] API 617 9th ed. Axial and Centrifugal Compressors and Expander-compressors

3

An Introduction to MapCycle Gas Turbine Integration Platform

Azizi, Rohollah
Bagheri, Mohsen
Mousavi, Fatemeh
Fatemeyi, SeyedHashem

MAPNA Turbine Engineering & Manufacturing Co. (TUGA)

Introduction

OEMs (Original Equipment Manufacturer) have always paid attention to developing their tools to simulate gas turbine performance and integrate it with other driven components, systems and sub-systems. This comes in particularly handy when designing new gas turbines, examining various control philosophies to optimize system performance, setting up gas turbine performance acceptance tests, Engineering projects and solving engineering problems.

Also as digital transformation and renewable energy are dramatically changing the future of equipment design and power-plant operation and maintenance, OEMs tend to focus on their performance algorithms to update them with the emerging risks or opportunities.

MapCycle is a performance integration platform that provides an accurate and up-to-date physical model of gas turbine integrated with auxiliary systems and components. To achieve the intended accuracy, main component characteristics should be obtained by combining the performance tests and performance tracking calculations in a sophisticated algorithm that gets the fleet data as input. System performance could be monitored to detect abnormalities and some specific recommendations could be provided by the physical and data-driven model. MapCycle modules are deployed in three software packages with their specific user interface for different clients. In addition, some of its modules are employed in TAPP[1] as TUGA CRM online system.

In this article, the main features of MapCycle platform for a simple cycle power plant are described.

[1] TUGA Application for Power Plant

MapCycle Workflow

TUGA, similar to the other big OEMs, intends to develop its own performance software -MapCycle- to fulfill the conventional requirements and overcome the new market challenges. The MapCycle workflow is designed to cover concepts like performance digital twin and condition monitoring, as well as big data technologies, online services for project engineering, interface with TAPP as TUGA CRM and offer solutions to other problems related to data and machine learning.

MapCycle is composed of independent but connected modules that shape a unified software with the aforementioned targets. As illustrated in Figure 1, these modules are:

- System Performance Integration Software
- Performance Tracking
- Performance Monitoring and Adviser
- Performance Test Software
- Database Management System
- User Interfaces

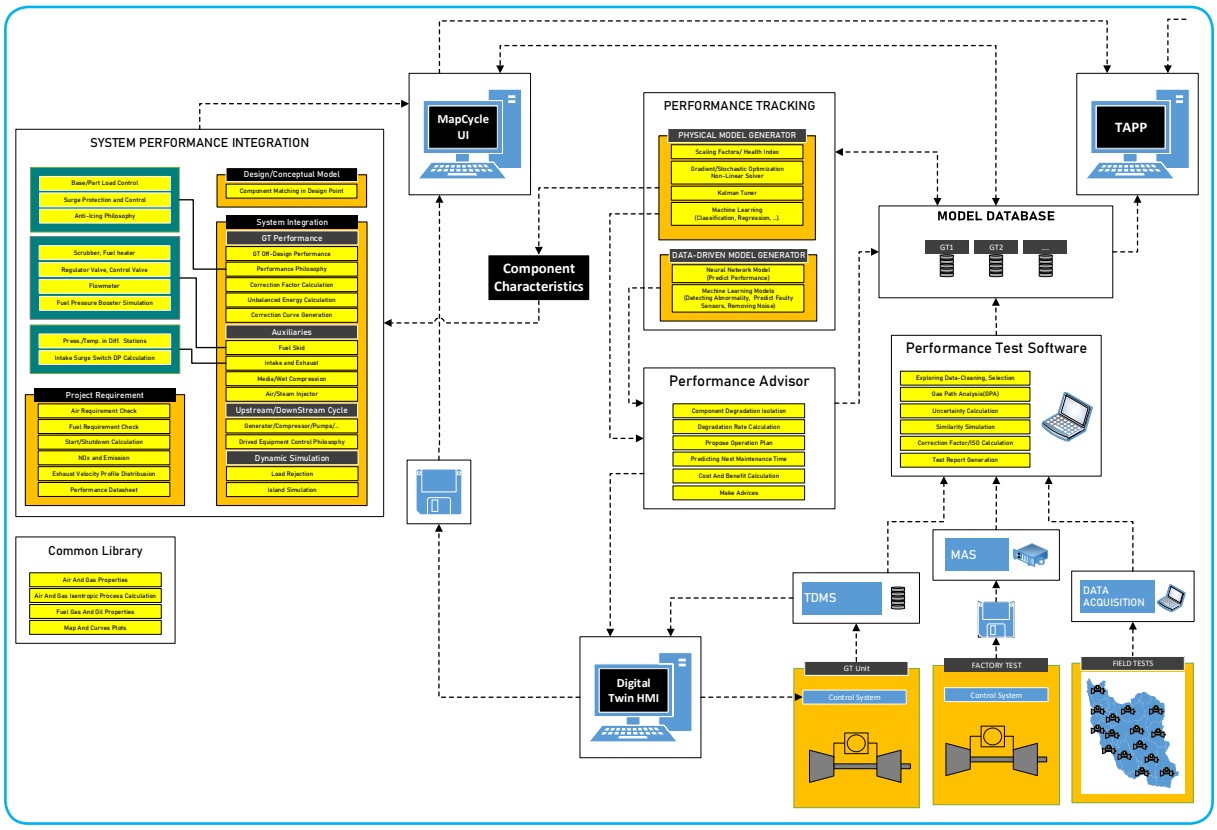

Figure 1 - MapCycle workflow

System Performance Integration

This module has been developing and has been being updated since 2015 with the initial aim of thermodynamic gas turbine simulation. It was developed in FORTRAN and was deployed in some simulators and testers. Coding has been switched to PYTHON since 2021 to take advantage of object-oriented programming.

The main considered capabilities for system performance integration are:

- Conceptual design of a new product including component matching, technology limits determination, scenario making and comparison
- Gas turbine simulation in different performance philosophies for base/part load: This means that this module can change some parameters like IGV and fuel mass flow in a pre-defined pattern to meet other parameters like the exit temperature and power. Philosophies include all the operation limits for max. power, anti-icing, pressure ratio, surge pressure difference, etc.
- Simulating standard fuel skid including scrubbers, control valves, flowmeters and customizing it by adding/removing heaters, pressure boosters, valves based on projects
- Simulation of intake and exhaust systems
- Simulation of media and Fog sub-systems
- Dynamic simulation of load rejection, island operation and fast IGV response
- Matching driven components like generator, pump and compressor with gas turbines and adding their performance philosophies

To perform these tasks, sophisticated codes were developed and used. The major inputs of these codes are the gas turbine components and equipment characteristic curves which are derived or modified from fleet/factory performance test data and digital twin for prototype test or performance monitoring. In this context, two software packages (i.e. performance test and performance tracking) were developed.

Performance Test Software

Performance test software is applicable to the fleet/factory acceptance performance tests. However, most of its modules are employed in digital twin and condition monitoring as well as component characteristic curve generation. This software works on the input performance data acquired from the gas turbine instruments. Its first task is exploring data to clean and find steady conditions based on the pre-defined permissible deviations. Then, GPA solves the balance of energy to calculate the key unmeasured parameters like turbine inlet temperature, air and gas mass flow rate, thermal efficiency, etc. Permissible deviations and GPA calculation are based on ISO-2314 or PTC-22 standards. Similarly, simulation for multi-shaft gas turbines to compute the extra information and correction factor computation to calculate the gas turbine performance in other desired conditions are among the next steps. Uncertainty of various parameters is derived from measured data, instrument uncertainty given in the laboratory certificates, and uncertainty algorithm. In the end, test report is generated automatically from the input data and computation results.

Performance Tracking

Performance tracking is a tool to generate the gas turbine component characteristics and other equipment like control valves. It also generates both physical and data-driven models for condition monitoring and fault diagnosis.

The physical model generator uses the performance test results and derives/updates

characteristic curves of gas turbine components. In prototype test of a new product, this tool returns to the component scaling factors applied on the initial map computed from CFD with the assumption of weak effects of tears and wears. Model generator optimizes the characteristic curves/surfaces -generated through Bezier method- by the gradient/stochastic optimizers to fit or approximate model results with the real data. For the upgraded gas turbine with the lack of data from prototype test, the fleet data provided in various performance tests are used as inputs.

The above-mentioned scale factors can be interpreted and changed to the health index for long-term condition monitoring in the gas turbine performance digital twin. Single point scaling, Kalman Tuner, nonlinear solvers and data analysis techniques are applied to compute the health indexes.

Data Driven model is another performance tracker that is applied for long-term monitoring of gas turbine. In this way, characteristic curves are not obtained, and the purpose is making a digital model of gas turbine only based on the measured data. For this, data analysis and some models of machine learning are employed for removing noises, predicting unmeasured parameters, detecting abnormalities, etc. A neural network model is also trained, evaluated and deployed to predict the performance. This model will be updated with the data-streams acquired from gas turbines.

Performance Adviser

Performance adviser initially uses the physical and data driven model to isolate degradation and calculate performance degradation rate. It is designed to produce technical service/ maintenance advice like online/offline washing, IGV tuning, etc. The main goals for performance adviser include predicting the remaining time to the next maintenance based on the different operation scenarios and proposing some plans and updating them to optimize the schedule for the next maintenance based on a cost and benefit analysis.

Database

As described in the previous sections, data is an integral part of performance tracking, updating models and making digital twins. These data are acquired from acceptance tests data acquisition system that is connected to the installed instruments and gas turbine Distributed Control System (DCS). In the factory test, data is transferred manually from DCS to MAS database. However, it is collected online and managed with an in-house developed software TDMS in the digital twin.

The most important database for performance tracking is called model database which contains:

- Performance test software outputs such as test reports, MOMs, calibration certificates, test experiences and GPA computation results
- Performance tracking outputs such as scaling factors, hyper-parameters of machine learning and deep learning models, component characteristics, etc.
- Performance advisor computation results such as degradation rates, proposed plan, remaining time to next maintenance etc.

Model database is just for the steady samples as described previously and the relation of samples with the raw data has been considered to generate it. A preliminary in-house database management program has been developed in Python for searching, manipulating, exploring and plotting purposes.

Software Applications

User Interface (UI) is the face of software, and the priority of MapCycle developing team is designing a user-friendly, modern and simple UI. Three pieces of software and their UI have been branched from MapCycle based on different clients' requirements including Web Application, Digital Twin and Desktop Software .

Web application is developed by TUGA software development team for the power plant Engineering and performing some routine calculations like:

- Datasheet calculation
- Fuel Gas/Oil composition analysis
- Estimation of GT performance at start/shutdown
- Correction factor calculation
- TET/TETC calculation
- General calculation
- Online performance acceptance test or maximum capacity test
- Generator capacity calculation

Digital Twin software has been developed in WINCC/C# for the industrial use, having fast response and other industrial standards as its development priority. MapCycle Desktop application is the most comprehensive software that includes all the previously described modules and would be developed in Django framework for the system performance experts.

Concluding Remarks

Software Platforms play essential role in the future of industries. They combine different technologies to make the modern and secure workflow and to offer custom-tailored products and services. In this article, the workflow of MapCycle platform and its main features including system performance integration, performance test software, performance tracking, performance adviser, database and software applications for a simple cycle power plant were described. Covering subjects of gas turbine design, project engineering and digital twin were the main goals in designing this platform. Handling and extracting values from big data through machine learning and artificial neural network formed the basis of this platform.

4

An Investigation into the Effect of Various Surface Post-Treatments on the Surface Condition of SLM-Printed Parts

Aliabadi, Mohsen
Ghodsi, Mahsa
Roozbahani, Behnam
Davarzani, Hossein

MAPNA Turbine Engineering & Manufacturing Co. (TUGA)

Introduction

Additive manufacturing is a complex and promising field that offers a wide range of merits, including the ability to design and produce components with intricate geometries, notably complex internal cavities and cooling channels. However, like any other technology, it presents some intrinsic challenges that must be navigated to meet the requirements of the targeted part. One of the most significant hurdles is achieving the surface roughness requirements of printed parts. The common strategy in the additive manufacturing industry is to separate the production process from the required post-processes for a desired surface roughness and consider them two independent steps. This approach toward the surface roughness of additively manufactured parts not only leads to achieving suboptimal surface conditions, but also causes an increase in the production cost of AM parts [1].

It is essential to consider the matter of surface roughness from the very initial steps of the manufacturing process. By doing so, several combinations of selecting items will be available, such as AM process parameters, manufacturing layer thicknesses, optimal process parameters regarding required surface quality, designed geometry, and building orientation. In choosing the appropriate post-processing techniques, factors such as feasibility and capability of the process (internal or external surfaces or simultaneously both), achievable surface roughness, material removal amount, accuracy, and process duration should be considered. The current research addresses these challenges and provides practical, effective solutions for optimizing the surface roughness in additive manufacturing.

Materials and Methods

In this survey, the required surface roughness samples were fabricated by Noura Layeh Negar M300 SLM machine; and Inconel 625 spherical powder with the nominal range of 15 to 53 microns was used as the feedstock material. The samples were produced using optimum process parameters. The layout of the printed samples on the building platform is shown in Figure 1(a). The printed samples were subjected to two surface related post processing treatments: sandblasting and vibratory surface finishing (VSF) in as-printed condition (without any subsequent heat treatment). The two mentioned post process treatments were carried out under a precise controlled condition utilizing optimum operating parameters. It is important to note that operating parameters in surface related post process treatments control not only the achieved surface quality, but also the amount of material removal.

For a comprehensive analysis, 12 samples were printed and post-treated in three different categories: as-printed (AP), sandblasted (SB), and vibratory surface finished (VSF). In order to investigate the effects of these treatments on each of the surface roughness creating factors, samples were printed with different angles toward the horizon (i.e. 90°, 60°, 45°, and 40°). After post processing treatments and before surface roughness measurements, samples were washed using an ultrasonic cleaning machine.

Surface roughness was measured using a non-contact scanner in a 5 mm ×5 mm surface area with ±1µm accuracy. The arithmetic average roughness (Ra) was measured to describe surface characteristics. Ra was calculated as the average of 4 measurements on different surface lines. For a better understanding of the process, a 3D view of scanned down-skin surface of the SB-40° sample is presented in Figure 1(b).

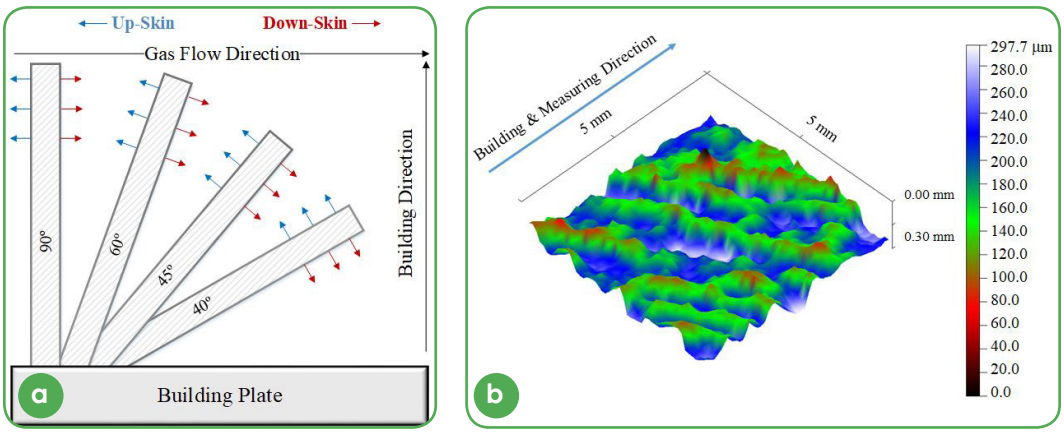

Figure 1 - (a) Layout of printed surface roughness samples on the building platform, (b) 3D view of scanned down-skin surface of SB-40° sample

The samples' thickness was meticulously measured with a high-precision digital micrometer, ensuring the accuracy of the measurements in each category to be aware of the material removal amount. To examine the topography of the samples' surfaces, stereo microscope (SM) equipment was used.

Results and Discussion

The average surface roughness parameter Ra for all surfaces is given in Table 1. At first glance, it is clear that both surface related post-treatments have improved the surface quality of the printed parts from the Ra value point of view. In addition, based on the results, it is evident that down-skin surfaces have worse conditions than up-skin ones. These findings underscore the importance of considering the orientation of the part during the additive manufacturing process, as it can significantly affect the surface roughness.

Table 1 - Results of surface roughness measurement for all types of surfaces

Sample Condition	Orientation	Ra (μm)			
		40°	45°	60°	90°
AP	Up-skin	10.4	8.4	7.4	7.4
	Down-skin	25.6	17.3	7.6	5.6
SB	Up-skin	5.9	3.7	4.2	4.4
	Down-skin	14.2	6.6	3.7	3.7
VSF	Up-skin	6.9	6.5	5.7	5.1
	Down-skin	15.0	8.3	5.8	5.4

Overall, the origin of roughness in various SLM printed parts with specific alloy powder, printer machine, and process parameters can be categorized into three cases: sintered and adhered powder colonies to the surface, staircase effect, and partial melting of powder at down-skin surfaces (sagging and dross formation defects). These cases are respectively related to the three factors: heat transfer issues, layer thicknesses, and overhangs. It is worth noting that the defects dross formation and sagging which occur due to overhangs, are slightly different. Dross formation is the partial melting of powder at down-skin surfaces. In contrast, in sagging defect, in addition to the partial melting of powders, the melt pool is lowered into the powder bed (formation of the vertical defect). Indeed, sagging is worse than dross formation created in samples with lower angles.

Based on Figure 2 (a), which illustrates the correlation between the angle of the sample with the horizon and the Ra values for AP samples for both up and up- and down-skin surfaces, in the AP-90° sample, the Ra value of up-skin surface is slightly higher than down-skin one, which is in contrast with the general mentioned pattern. For 90° samples, the definition of up and down-skin surfaces is meaningless, and the observed difference in the Ra values of these two surfaces is related to the argon gas flow direction in the building chamber. It is important to note that the gas flow direction is directly related to heat transfer. According to the figure, the Ra value increases as the sample angle decreases. The observation resulted from the simultaneous effect of two factors, namely staircase and overhang effects. It is important to note that sintered and adhered powder colonies significantly impact roughness on all printed surfaces. Although, it seems that this factor plays a less significant role than the other factors mentioned above. Throughout this investigation, due to the approximate geometrical similarity of the printed samples to each other, the effect of this factor has been considered the same for all samples.

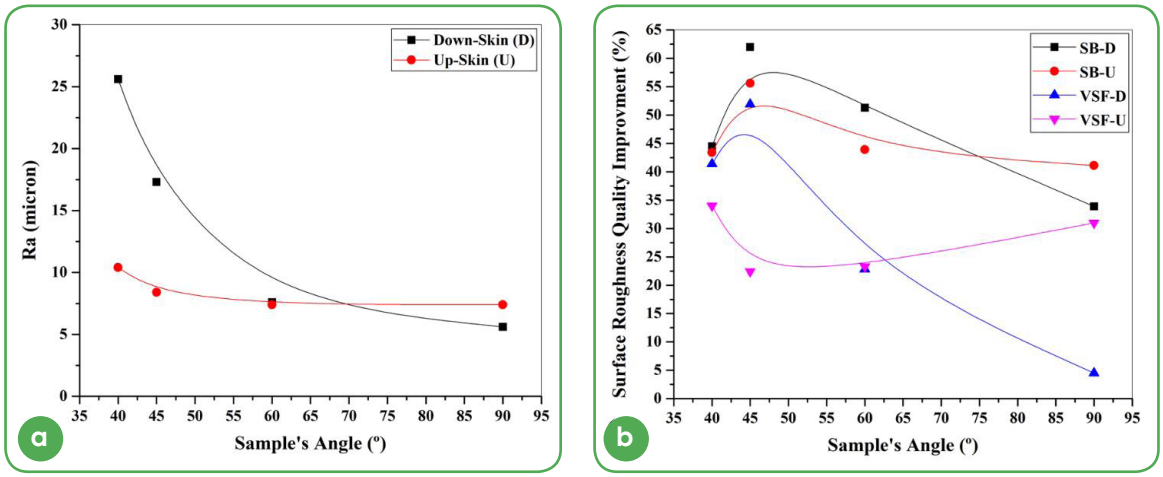

Figure 2 - (a) Surface roughness characteristic (Ra) of AP samples, (b) Surface roughness quality improvements of SB and VSF samples

SM images of AP samples from both up- and down-skin surfaces are presented in Figure 3. Except for the adhered sintered powder colonies to the surface, it is clear that in up-skin surfaces, the only influential roughness-creating factor has been the staircase effect; while in down-skin surfaces, both factors of staircase and dross formation are influential. However, according to Figure 3, dross formation and subsequent sagging defect formation have a much more decisive role in the latter surfaces. Figure 3 also reveals that the staircase effect leads to the surface roughness increment of up-skin surfaces at samples with angles less than 45°, while this angle for down-skin ones is 60°.

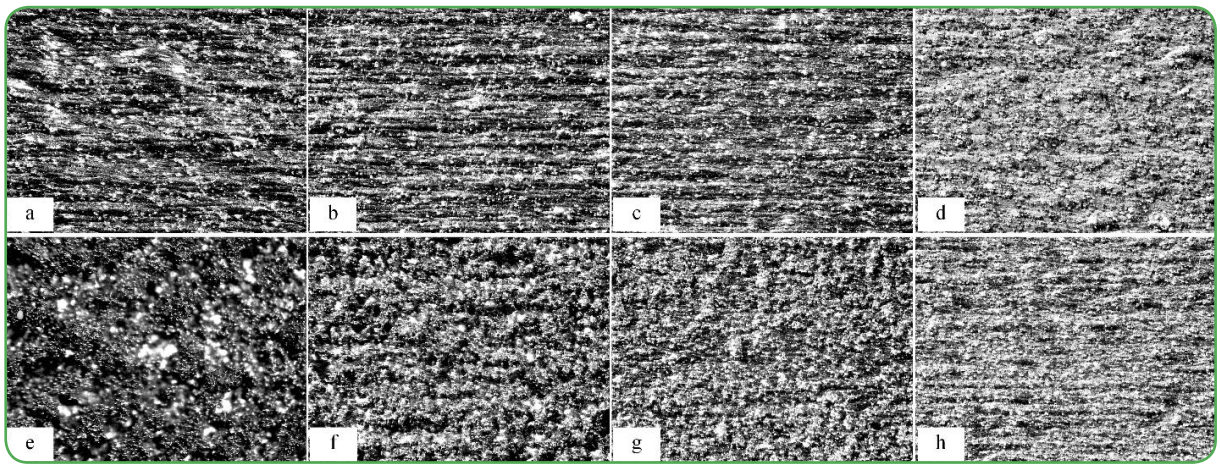

Figure 3 - SM images of AP samples from both up-skin (a-d) and down-skin (e-h) surfaces at various angles toward the horizon, (a & e): 40°, (b & f): 45°, (c & g): 60°, (d & h): 90°

The average percentages of surface roughness improvements after performing two surface finishing-related post processes, sandblasting and VSF (in comparison with the as-built condition), are presented in Figure 2 (b). As can be seen in the figure, the sandblasting process has had a more positive impact than the VSF process on surface quality improvements, which is compatible with the SM images of SB and VSF samples (Figures 4 & 5).

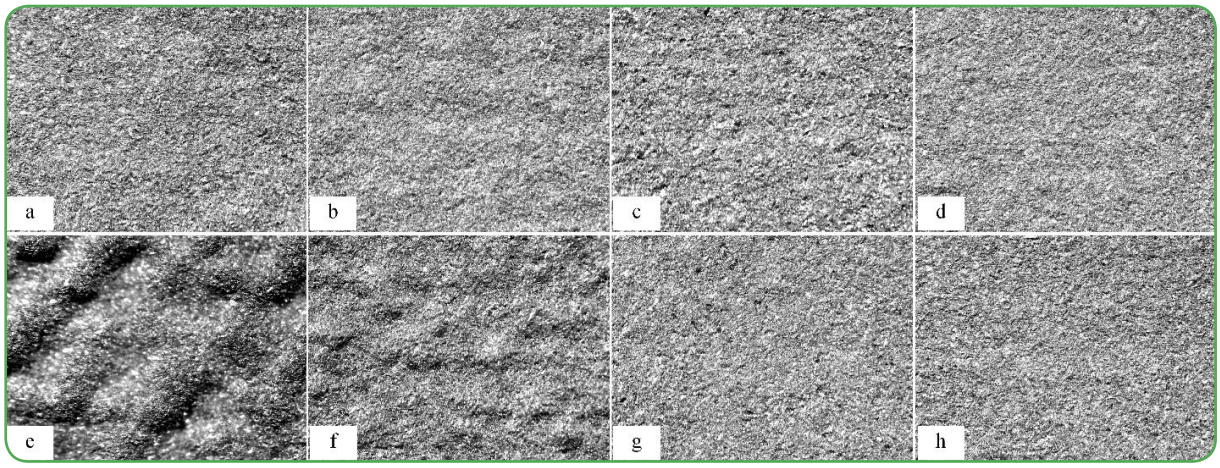

Figure 4 - SM images of SB samples from both up-skin (a-d) and down-skin (e-h) surfaces at various angles toward the horizon, (a & e): 40°, (b & f): 45°, (c & g): 60°, (d & h): 90°

It is important to note that factors, such as material and properties of printed parts and the process parameters used in manufacturing and post-processing treatment steps should be considered when investigating the effects of various post-treatments. Additionally, it is concluded that both performed surface related post process treatments had a more significant effect on down-skin surfaces. In other words, post processing has played a more important role on surfaces with the rougher conditions. Based on the mentioned pattern, it is predicted that a higher improvement will be achieved at samples with angles of 40° and 45° for each sample's condition, which is in complete agreement with the observed trend.

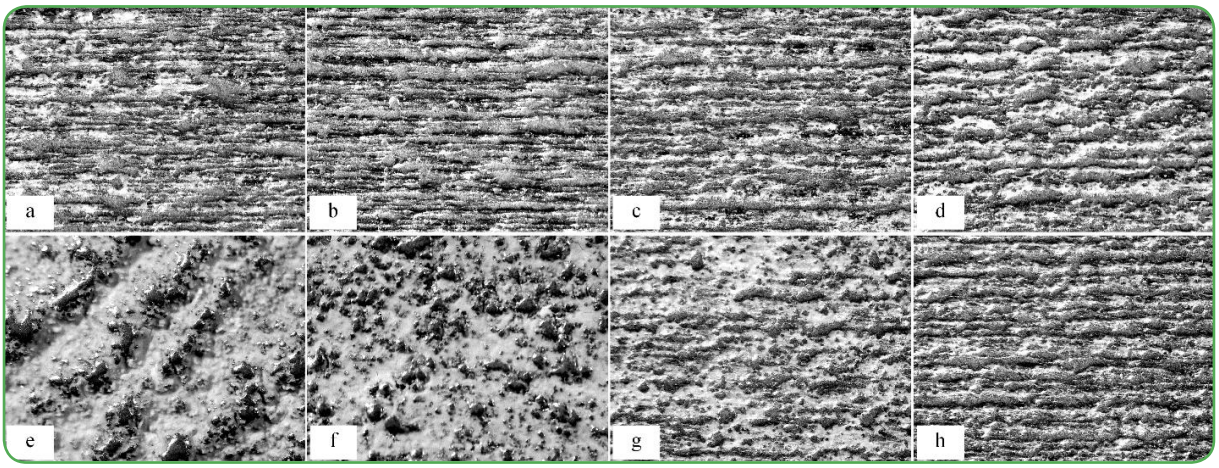

Figure 5 - SM images of VSF samples from both up-skin (a-d) and down-skin (e-h) surfaces at various angles toward the horizon, (a & e): 40°, (b & f): 45°, (c & g): 60°, (d & h): 90°

Figure 2 (b) shows that on down-skin surfaces, the highest impact of post process treatments was achieved at samples with an angle of 45°. Indeed, at samples of 40°, sagging defect occurs due to an inappropriate (too low) angle at overhangs, and none of these two post-process treatments could eliminate them. In other words, at these surfaces and angles of 45°, a dross formation defect is created, and both surface treatments could cope with it. Another interesting point is that the pre-mentioned pattern can be observed regarding up-skin surfaces in only SB samples. Based on the comparison of SM images (related to the up-skin surfaces) it is clear that the sandblasting process can eliminate stairs resulting from the staircase effect. Although the capability of the VSF process has been more limited than the sandblasting process, it has just been able to omit the sintered and adhered powder colonies to the surface and consequently has improved the surface quality in this way. Based on this fact, it can be interpreted that in the sample of 45°, the influences caused by the staircase effect (as a result of the sample's angle toward the horizon) have been at a level that the sandblasting process was able to remove the roughness-creating factor completely. Although by reducing the sample's angle from 45° to 40°, and subsequently the increment of the staircase effect, the sandblasting process was not sufficient to completely eliminate the roughness-creating factors. Therefore, the most significant impact occurred in the 45° sample. Nevertheless, in the case of VSF samples, because the process was only capable of removing adhered powder colonies on the surface (not the surface's stairs), and also based on the fact that at up-skin surfaces of the sample of 40° there are more amounts of partially melted powders (based on SM images), the most outstanding effect was observed.

The fact stated about the ability of the performed sandblasting and VSF process on the printed parts regarding removing surface roughness creating factors, is verified by Figure 6. By reducing the angle of the parts and consequently creating stairs and areas with partially melted powders on the surface, an increasing amount of material reduction has occurred in the sandblasting process. However, the VSF process can only remove sintered powders on the surface. Therefore,

no difference can be observed by changing the angle of the sample. It should be noted that the cases and results stated in this research are verifiable for samples printed with Inconel 625 alloy in as-printed condition, with a hardness of 320 Vickers. In other words, if samples made with an alloy with lower hardness and better workability are examined, different results will be obtained. For instance, it is mentioned in the literature [2] that by performing the VSF process on the printed samples of alloy 316, the elimination of surface profile peaks and also a work-hardened layer with increased micro hardness values at surface and subsurface areas are achieved; something that did not happen in this research, because of the high hardness of the used samples.

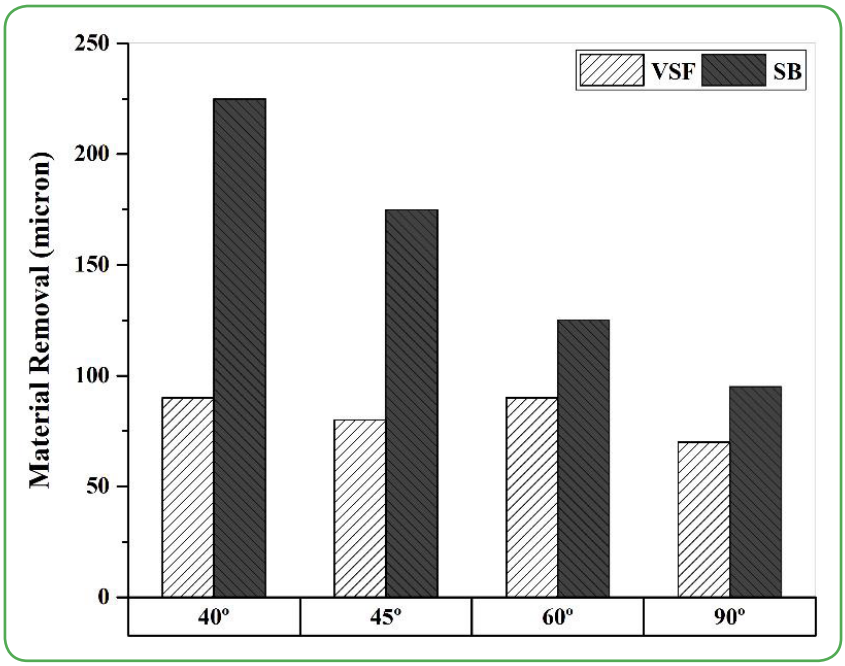

Figure 6 - The difference in samples' thickness quantities after sandblasting and VSF post processes

Concluding Remarks

The surface roughness issue of additively manufactured parts is one of the most challenging problems that needs to be dealt with to obtain high-quality components. It is essential to pay attention to the fact that considering this issue from the very beginning of the part production is instrumental from both quality and cost viewpoints. Based on this survey, VSF and sandblasting post-process treatments are two readily available, effective, and cost-efficient processes that can be used for surface quality improvements. However, their limitations, such as not being suitable for the part's internal channels and minimum achievable surface roughness, shall be considered when selecting the proper post-process treatment.

References

[1] Binder, Robert, et al. "*Smooth Surfaces for Additive Manufacturing*", EOS Whitepaper (2018).

[2] Nezarati, Masoud, et al. "*The effect of the vibratory surface finishing process on surface integrity and dimensional deviation of selective laser melted parts.*" Proceedings of the Institution of Mechanical Engineers, Part B: Journal of Engineering Manufacture (2023).

5

Investigating Metallurgical Aspects of Repair Welding of Cr-Mo Low Alloy Steels

Ebrahimian, Ali
Rezazadeh, Hossein
Fathi, Alborz

MAPNA Turbine Engineering & Manufacturing Co. (TUGA)

Introduction

Contrary to their interesting advantages, welding of Cr-Mo low alloy steels is associated with reduction in toughness, and susceptibility to reheat cracking [1],[2]. Welding of these steels causes metallurgical changes in the heat-affected zone (HAZ) and downgrades the mechanical properties of the joint. Improving the microstructure and mechanical properties of the joint requires post weld heat treatment (PWHT) and use of appropriate fillers. However, implementation of PWHT at high temperatures for most low-alloy steels can cause distortion [3]. In some repairs such as that of huge parts, PWHT is considerably challenging, costly and time-consuming because of safety considerations, cleaning, disassembly, protection of adjacent machinery, bracing/clamping, heating/cooling setup, and reassembly [3]. Thus, it is favorable to explore alternative techniques that eliminate PWHT and diminish risk of distortion, cut time and expenses, make on-site repair possible, and consequently reduce facility outage time and overhaul cost.

Challenges of Cr-Mo Steels Welding

■ Toughness reduction in coarse grain HAZ (CGHAZ)

Due to temperature raise to much higher than A_{C3} in the areas close to melting zone, an increase in the dissolution of grain boundary precipitates, intense diffusion and grain growth, and grain sizes in these areas is observed. This in turn, causes a decrease in toughness due to the reduction of grain boundaries as barriers to crack propagation.

■ Impact energy reduction in inter-critical HAZ (ICHAZ) and inter-critical coarse-grained HAZ (ICCGHAZ)

Partial dissolution of microstructure into austenite occurs at grain boundaries in that portion of base metal (ICHAZ) or previous welding passes (ICCGHAZ in multi-pass welding) that experience maximum temperature in the range of A_{C1}-A_{C3} during welding. As a result, martensite-austenite (M-A) particles rich in carbon (more than 0.5 weight percent) and strong carbide-formers, which were already rejected into austenite, can be formed in ICHAZ/ICCGHAZ during cooling and reduce fracture toughness [4]. Brittle M-A islands in which martensite has a twinned substructure and the volume fraction of martensite can reach 96-97%, are normally placed along the primary austenite grain boundaries [3] and are a major contribution to reduction in ductility [4].

■ Hydrogen Induced Cracking (HIC)

Cr-Mo steels are commonly susceptible to hydrogen cracking due to their relatively high hardness, and if other conditions are met (high residual stress, hydrogen dissolution) at low temperatures and especially for heavy sections, hydrogen cracking may occur in these steels.

■ Reheat Cracking

Reheat cracks are intergranular cracks (Figures 1 and 2) which can appear in weld or coarse HAZ of Cr-Mo or Cr-Mo-V steels due to reheating or service in the temperature range of 350 to 550°C [5]. As a result of being heated, the areas adjacent to the grain boundaries are depleted of elements that cause solution hardening which when combined with carbon and other impurities stipulate temper embrittlement, and form a network of brittle compounds at grain boundaries. In-service or residual stresses cause severe strain concentration in the adjacent areas to grain boundaries. Along with the presence of brittle compounds at the grain boundaries, intergranular cracks nucleate at impurity-matrix interfaces and propagate [6].

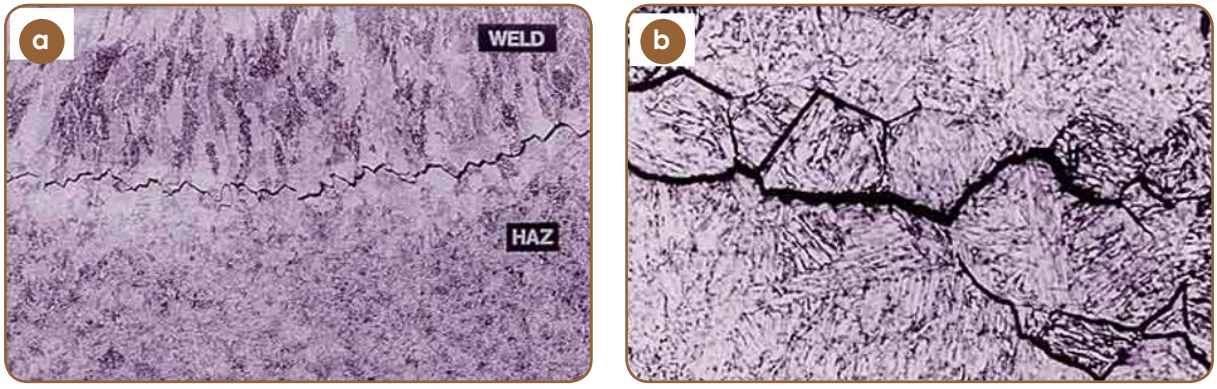

Figure 1 - a) Reheat cracking in CGHAZ, b) Intergranular morphology of reheat cracks [7]

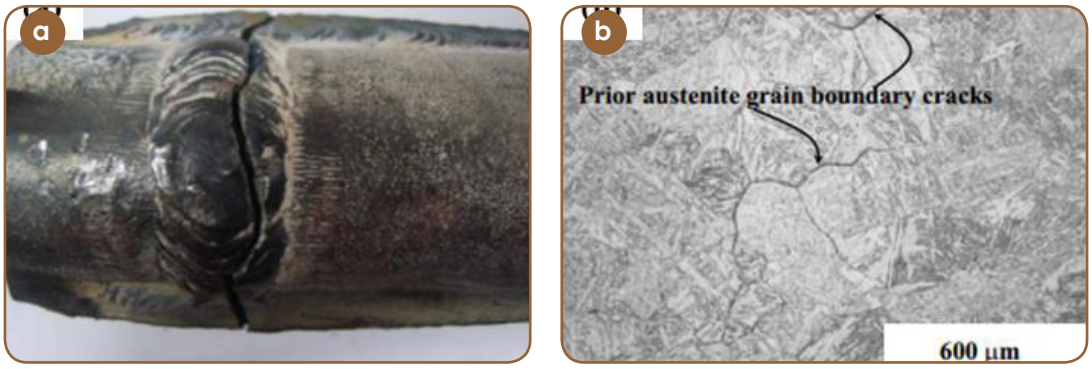

Figure 2 - Reheat cracks in the weld metal of a T23 steel tube in a fossil fuel power plant: a) image of the damaged tube and b) optical microscope image of microstructure in the damaged region of the tube [8]

High temperature, high stress and base metal susceptibility to reheat cracking, when combined, cause cracking mainly in HAZ. So far many indices have been defined based on chemical composition to determine the sensitivity limit of steels to reheat cracking [7]:

$$\Delta G1 = 10C + Cr + 3.3Mo + 8.1V - 2$$

$$P_{SR} = Cr + Cu + 2Mo + 10V + 7Nb + 5Ti - 2$$

$$Rs = 0.12Cu + 0.19S + 0.10As + P + 1.18Sn + 1.49Sb$$

Steels having a value of ΔG1 of less than 2, P_{SR} less than zero or Rs less than 0.03 are less susceptible to reheat cracking. The value of ΔG1 for the steel studied in this research is 5.94, which shows possible susceptibility to reheat cracking. The amount of in-service or residual stresses in welded joints plus coarse grain are other factors being regarded as design, construction and performance attributes.

■ Experimental design and project plan

PWHT of in-service or finished parts with tight tolerances and high residual stresses is challenging due to the likelihood of distortion. PWHT of parts whose persistent function is vital is also inconvenient. As a result, it is necessary to find alternative techniques to PWHT. This article focuses on appropriate solutions to eliminate PWHT. The idea originated in repair welding of stop/control valve seats of steam and gas turbines (Figure 3) exposed to corrosion, erosion and cavitation [9]. The following methods were proposed for welding 21CrMoNiV4-7+QT steel, which is the material used in MST-50 steam turbine stop/control valve:

1. GTAW with ERNiCr-3 filler wire without PWHT
2. SMAW with E9018-B3 electrode and PWHT
3. SMAW by Temper Bead technique (TBW) [10] with E9018-B3 electrode

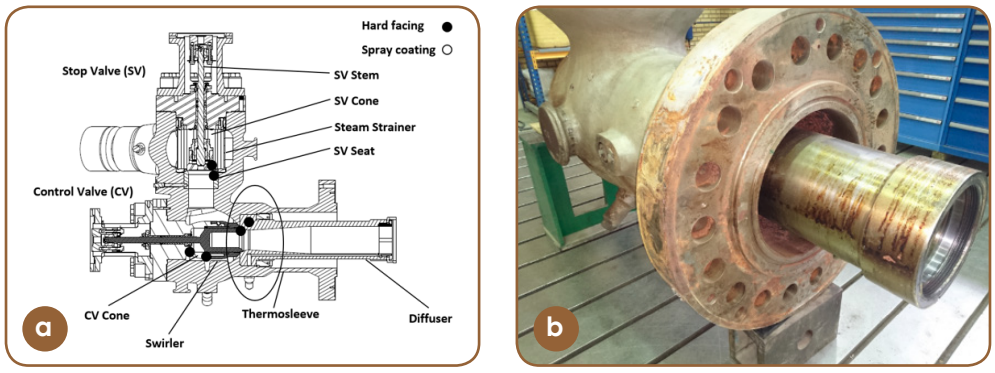

Figure 3 - (a) Cross section of a valve marking seats by black curves [9], (b) a stop/control valve

To investigate the effect of changing the filler type on the possibility of eliminating PWHT, nickel-based filler was used. The effects of each method on the mechanical properties of the welded joints are examined and quantitatively evaluated as follows.

Test Materials and Methods

21CrMoNiV4-7+QT steel was used in the form of 40 mm thick sheets cut from a 300 mm diameter steel bar. The nominal chemical composition and mechanical properties of this steel are given in Tables 1 and 2. To prepare test plates, a groove was machined in every sheet according to Figure 4(a).

Table 1 - Nominal chemical composition of 21CrMoNiV4-7+QT steel (weight percent)

C	Si	Mn	S	P
0.17 - 0.25	0.15 - 0.35	0.35 - 0.85	≤ 0.020	≤ 0.020
Cr	**Mo**	**Ni**	**V**	**Al**
0.9 - 1.2	0.65 - 0.80	0.5 - 0.8	0.25 - 0.35	≤ 0.015

Table 2 - Mechanical properties of 21CrMoNiV4-7+QT steel

Yield strength (MPa)	Tensile strength (MPa)	Elongation (%)	Reduction of area (%)	Impact energy (J)	Hardness (HB 30)
550-700	≥ 700	≥ 15	≥ 40	≥ 24	≥ 215

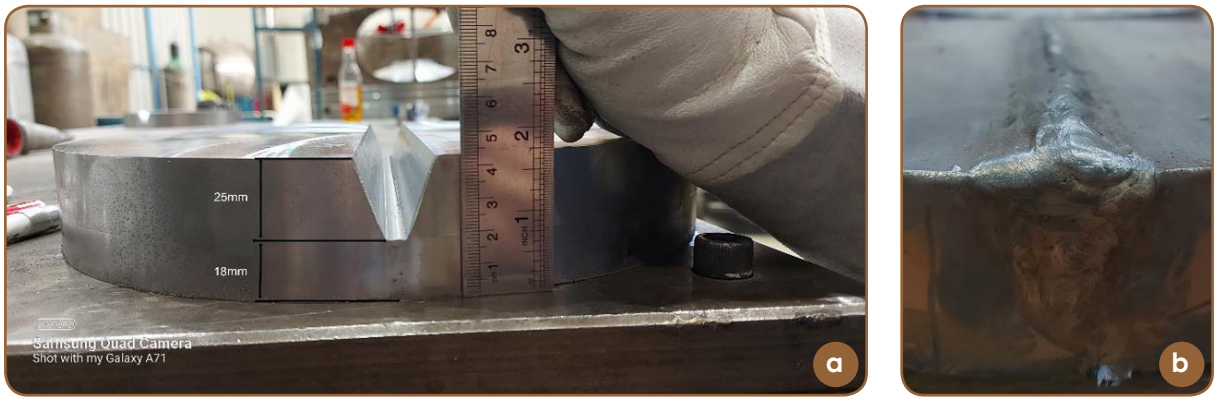

Figure 4 - (a) Dimensional specifications of test plates, (b) One typical completed test plate

Welding was done as shown in Figure 4(b) according to the specifications shown in Table 3. The chemical compositions of filler and electrode are given in Table 4. In the second method, two buttering layers were applied before welding (Figure 5).

Table 3 - Welding parameters

Welding technique	Process	Current (A)	Voltage (V)	Polarity	Mean travel speed (mm/min)
No PWHT-ERNiCr-3	141	150 - 200	11 - 14	DCEN	105
PWHT-E9018-B3	111	120 - 145	19 - 22	DCEP	185
TBW-E9018-B3	111	165 - 180	20 - 24	DCEP	145

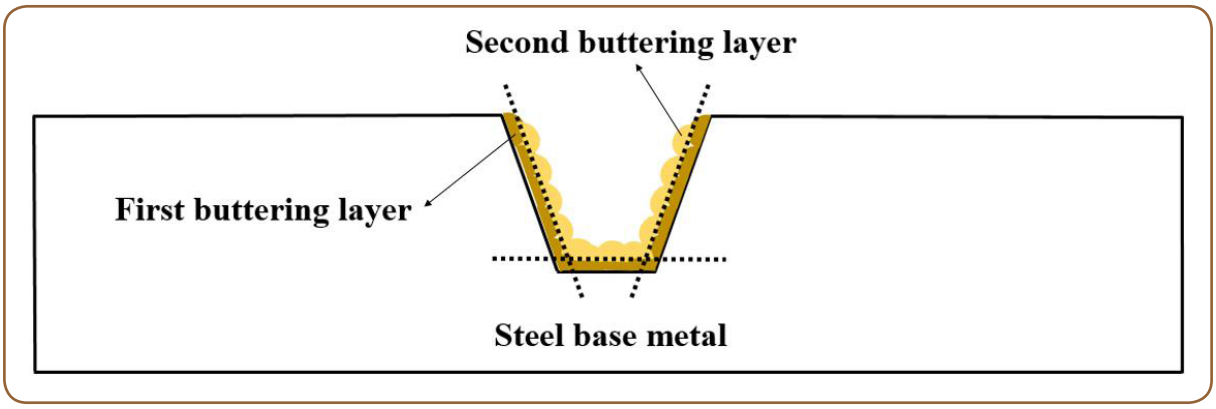

Figure 5 - Schematic of buttering in TBW sample

After the visual inspection of the welds, the test plates were inspected by penetrant liquid testing (PT) and radiography testing (RT) and their soundness was confirmed. PWHT was performed for the third sample as illustrated in Figure 6. Transverse tension at ambient temperature, impact, hardness measurement, macrography and micrography were performed.

Table 4 - Chemical composition of the filler and electrode (weight percent)

Filler/ Electrode	C	Si	Mn	Cr	Mo	P	Nb	Fe	As	Sb	Sn	Ni
ERNiCr-3	0.02	0.1	3.1	20.5	-	-	2.6	≤1	-	-	-	Balance
E9018-B3	0.08	0.3	0.8	2.3	1.0	≤0.010	-	-	<0.005	≤0.005	≤0.005	-

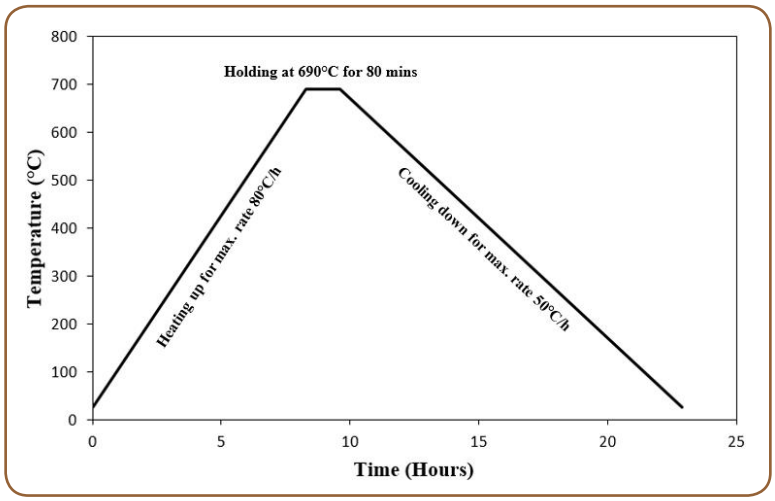

Figure 6 - Schematic representation of PWHT cycle

Results and Discussion

■ Microstructural observations

Macroscopic images of the joints cross-sections in Figures 7-9 depict that except for the PWHT sample in which a lack of fusion (LOF) is observed in the root (Figure 7), the sample produced by TBW (Figure 8) shows many interpass LOFs in the weld. The nickel-based filler joint (Figure 9) was welded without any visible defects. There are no evidences showing the presence of reheat cracks.

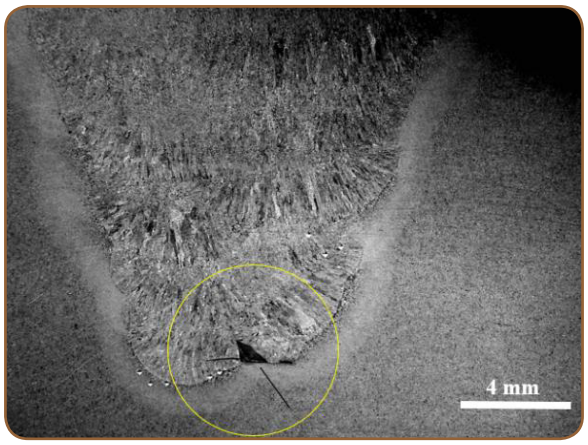

Figure 7 - Macrographic image of the PWHT sample. The marked area indicates the location of a defect in the root

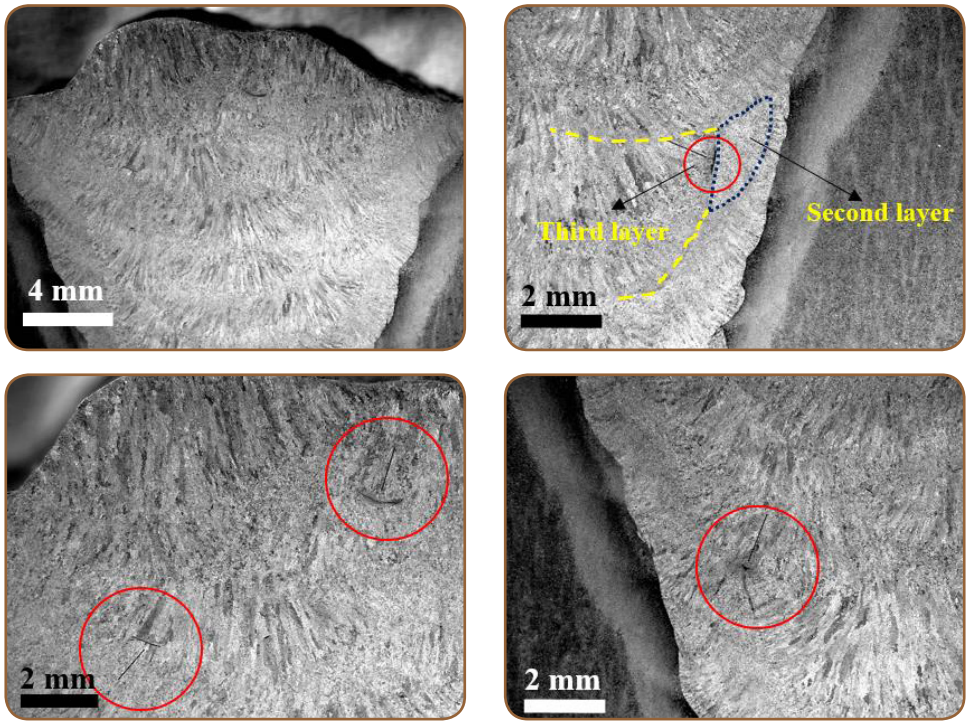

Figure 8 - Macrographic image of the weld of the TBW sample. The circles on the figure show the locations of interpass LOFs

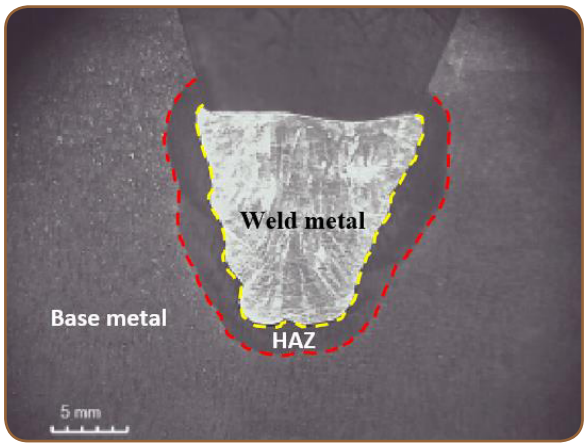

Figure 9 - Macrographic image of the weld in the nickel-based filler sample

The base metal micrograph shown in Figure 10, indicates that the refined microstructure of the base metal is mainly composed of tempered lath martensite.

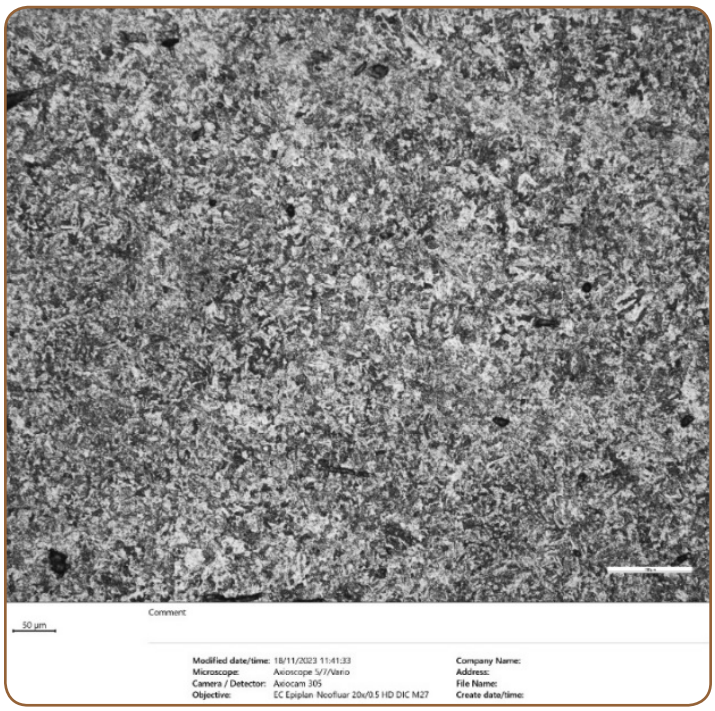

Figure 10 - Optical microscope image of the base metal showing quenched and tempered microstructure

Figures 11 and 12 show the HAZ microstructure of the PWHT and TBW samples, respectively. The samples were etched under the same conditions of temperature and time. While in the TBW sample it is easy to determine the interface of HAZ and base metal, for PWHT sample, even the border between HAZ and base metal is hard to identify owing to the tempering of both the base metal and HAZ. It is inferred that the HAZ microstructure of PWHT sample is tempered to a greater extent.

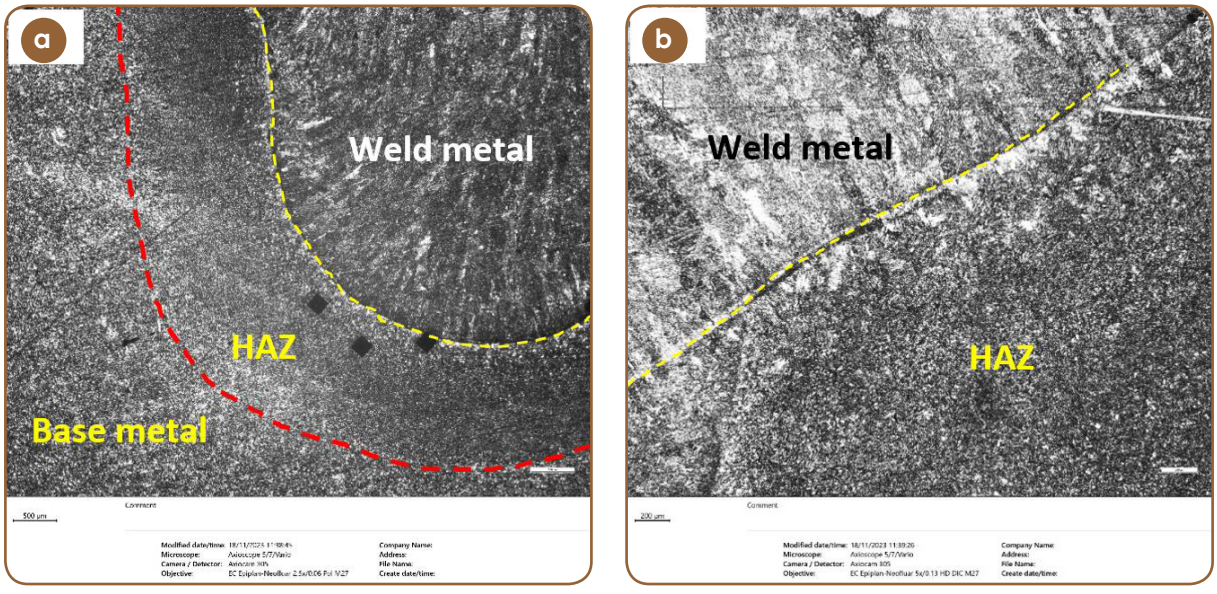

Figure 11 - Optical microscope image of the HAZ of the PWHT sample, (a) in low magnification and (b) in higher magnification

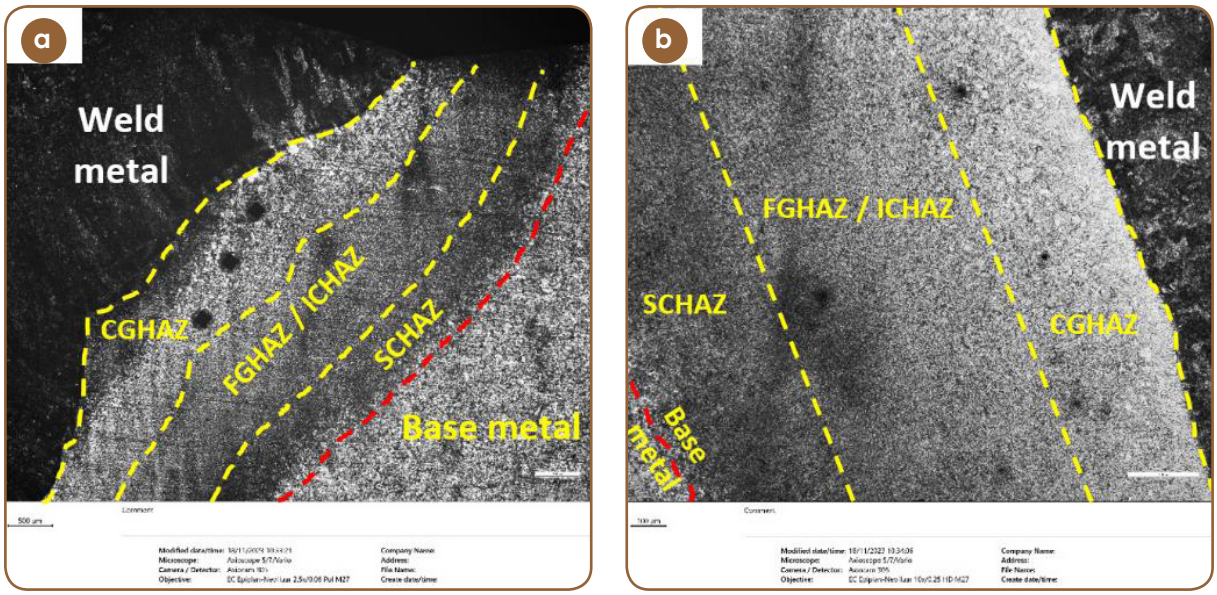

Figure 12 - Optical microscope image of the HAZ of the TBW sample, (a) in low magnification and (b) in higher magnification

As Figure 13 shows, by tempering, carbon precipitates from supersaturated BCT[1] martensite as carbide particles of iron and carbide-formers at primary austenite or lath martensite grain boundaries [11].

After etching, carbides/martensitic matrix interfaces are corroded, overlapping and appearing as dark areas in the micrographs (Figure 13). Deposition of carbide particles at primary austenite and lath martensite grain boundaries are depicted in Figure 14. With increase of tempering time, the darkness of the optical microscope images of a tempered martensitic microstructure gradually increases. This has caused more darkness in the optical microscope images of PWHT samples compared to TBW samples or more darkness in the SCHAZ compared to FGHAZ/ICHAZ and CGHAZ of TBW samples (Figures 11 and 12).

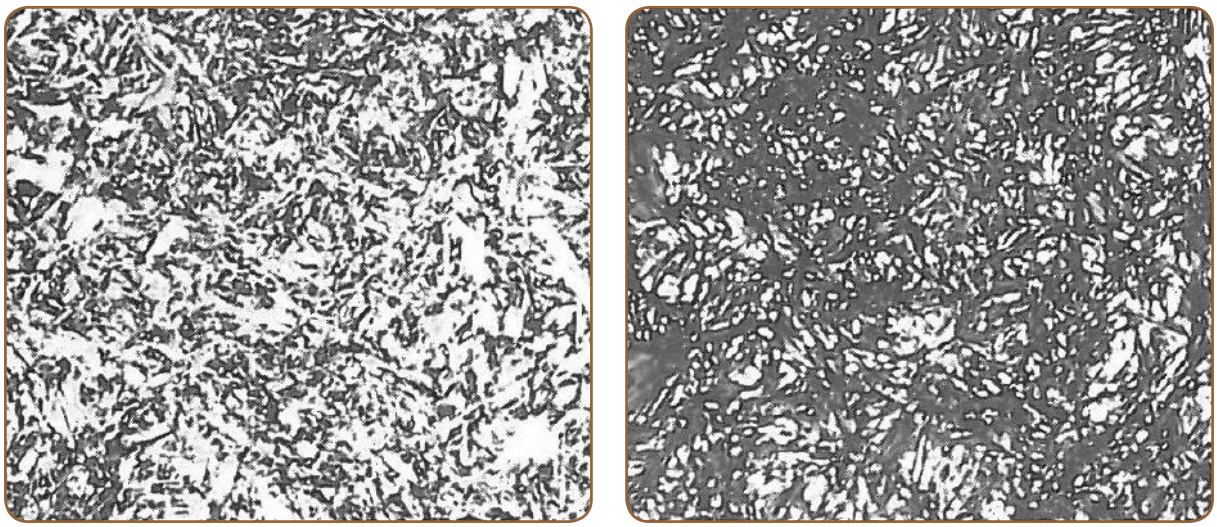

Figure 13 - Left image: microstructure of 1095 steel, austenitized at 816°C and quenched in water. The microstructure includes untempered lath martensite and a number of carbide particles, right image: the same steel with the same heat treatment tempered at 149°C. The microstructure includes tempered martensite (darker than the image on the left) and a number of carbide particles [11]

[1] Base Centered Martensite

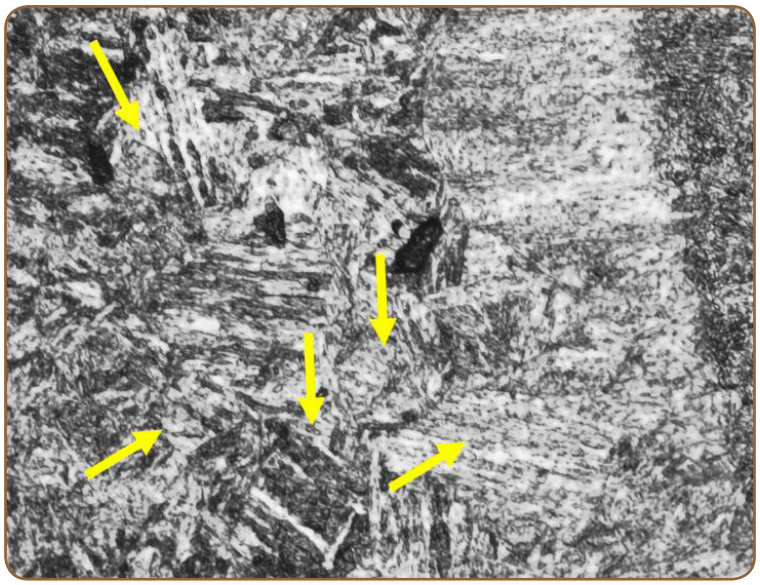

Figure 14 - Optical microscope image of the tempered lath martensite microstructure in the HAZ of the heat treated sample.

Figure 15 shows the microstructure of the weld in PWHT and TBW samples. The casting structure with columnar grains is clearly evident, especially in the TBW sample. The microstructure of PWHT sample has been tempered more than that of TBW sample due to applying heat treatment.

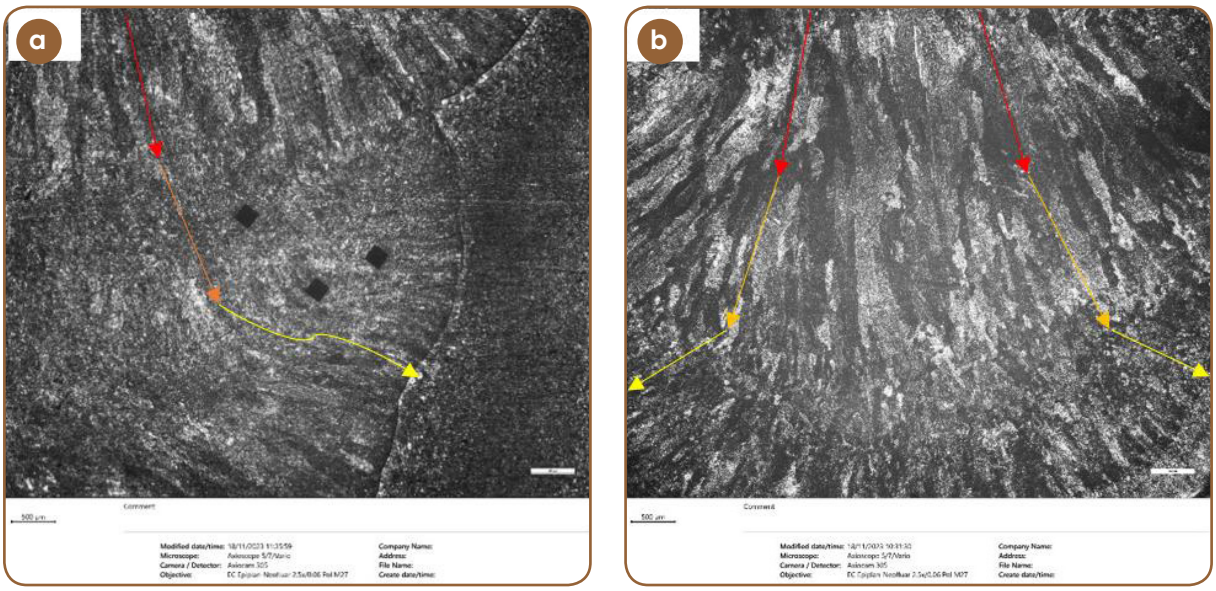

Figure 15 - Micrograph of the weld and growth direction of columnar grains in (a) PWHT samples, and (b) TBW samples.

■ Mechanical properties

The mechanical properties of all welded samples were investigated from the perspective of mechanical strength, impact energy and hardness.

Table 5 summarizes the results of mechanical tests. In general, the mechanical properties of all samples meet the minimum requirements stated in the material specification. The ultimate strengths of the nickel-based electrode and TBW samples are almost similar and higher than that of PWHT sample. The lower tensile strength of PWHT sample is related to more tempering

due to PWHT. This phenomenon has caused the hardness of PWHT sample to be lower than the TBW sample, both in the HAZ and weld.

While it was expected that the weld hardness of TBW sample would be similar to that of PWHT sample because of the tempering effects of successive passes in TBW, this did not occur. Comparison of the impact energy values shows that, as expected, while the weld toughness in the nickel-based joint is higher than that of other samples, the weld toughness of PWHT sample is about 2 times greater than that of the TBW sample.

Mechanical test results are consistent with the microstructural observations and show that the parameters set for TBW have not led to as much increase of heat as in the PWHT sample. Thus, the weld and HAZ tempering rate have not been sufficient to reduce the hardness. With this setting, welding cannot be performed without PWHT if a balance of strength and toughness is expected. It is necessary to increase heat input by increasing current and/or decreasing welding speed which in turn, makes the process energy/time-consuming for repairing large defects.

Table 5 - Mechanical properties of the welded joints

Welding condition	PQR No.	Hardness (HVN)		Ultimate strength (MPa)	Impact energy (J)	
		Weld metal	HAZ		Weld metal	HAZ
No PWHT-ERNiCr-3	126	215	450	749 - 785	200	163
PWHT-E9018-B3	127	242	302	723 - 723	119	224
TBW-E9018-B3	128	303	431	764 - 773	61	153

Performances of the methods are compared in Table 6. From the standpoint of proportionality of welding method and defect size, welding with nickel-based electrode, TBW and with PWHT are suitable for repairing small, medium-sized and large defects, respectively.

Table 6 - Performance comparison of the welding techniques

Welding technique	Need for PWHT	Practicality of on-site welding	Weld/base CTE[2] mismatch	Defect size
No PWHT-ERNiCr-3	No	No	High	Small
PWHT-E9018-B3	Yes	Relatively	Low	Large
TBW-E9018-B3	No	Yes	Low	Medium

Welding with nickel-based filler is prone to generate high thermal and residual stresses because of the difference in CTE between weld and base metal. Regarding the TBW, the evidences show that the heat input is not high enough to remove PWHT to repair large defects. It is necessary to perform PWHT for repairing large defects. But regarding repair welding of medium-sized defects, welding can be done with TBW.

[2] Coefficient of Thermal Expansion

Concluding Remarks

To investigate the possibility of eliminating PWHT to reduce repair time, equipment outage time and reduction of welding operations cost, a study was carried out in TUGA in which the effect of welding with nickel-based filler, TBW, and welding with PWHT on mechanical properties of the samples were compared.

As the TBW sample is tempered to much lower extent in comparison to PWHT sample, increasing current and decreasing welding speed can result in a balance between strength and toughness. Furthermore, tensile strength of TBW and nickel-based filler samples were higher than that of PWHT sample. Although nickel-based filler and TBW samples presented the weld highest and lowest impact energies, respectively, PWHT sample marked the highest HAZ toughness in comparison to nickel-based filler and TBW samples.

It was deduced from the results that the best methods to repair small, medium-sized and large defects, were to weld using nickel-based filler, TBW, and welding with PWHT, respectively. This means that parts with small and medium-sized damages can be restored without PWHT.

References

[1] C. a. J.-P. S. Chovet, *"Additional recommendations for welding Cr-Mo-V steels for petrochemical applications,"* vol. 55, 2011.

[2] C. a. P. S. Chauvy, *"Prevention of weld metal reheat cracking during Cr-Mo-V heavy reactors fabrication,"* 2009.

[3] Z. Odanović, *"Some advanced welding technologies applied for repair welding in power plants,"* vol. 27, no. 4, 2021.

[4] D. B. N. K. J. H. P. a. O. A. Farichild, *"A study concerning intercritical HAZ microstructure and toughness in HSLA steels,"* vol. 70, no. 12, 1991.

[5] N. C. J. a. K. S. Heo, *"Elevated temperature intergranular cracking in heat-resistant steels,"* vol. 559, 2013.

[6] H. H. N. a. K. S. Sung, *"Intergranular Cracking Susceptibility of 2.25 Cr Heat-Resistant Steels Depending on Alloying Elements and Impurities,"* vol. 47, 2016.

[7] [Online]. Available: twi-global.com/technical-knowledge/job-knowledge/defects-imperfections-in-welds-reheat-cracking.

[8] N. C. J. Y. K. L. J. a. K. J. Heo, *"The mechanism of elevated temperature intergranular cracking in heat-resistant alloys,"* vol. 528, no. 6, 2011.

[9] S. S. A. B. J. W. D. a. S. H. Brussk, *"Steam turbine valve hard-facings: experience and latest developments,"* Turbo Expo: Power for Land, Sea, and Air, vol. 45585, 2014.

[10] H. Rezazadeh, *"Evaluation of the efficiency of temper bead technique for repair welding of Chromium-Molybdenum alloy steel parts,"* Technical Review, pp. 31-36, 2022.

[11] G. F. S. R. L. B. R. S. G. J. A. C. P. J. K. K. M. S. D. H. a. W. W. S. J. Vander Voort, ASM Handbook, Metallography and microstructures, vol. 9, ASM International, 2004.

[12] S. a. T. H. Aihara, *"Influence of high-carbon martensitic island on crack-tip opening displacement value of weld heat-affected zone in HSLA steels,"* vol. 39, no. 10, 1987.

Head Office:
231 Mirdamad Ave. Tehran, I.R.Iran.
P.O.Box: 15875-5643
Tel: +98 (21) 22908581
Fax: +98 (21) 22908654

Factory:
Mapna blvd., Fardis, Karaj, I.R.Iran.
Post code: 31676-43594
Tel: +98 (26) 36630010
Fax: +98 (26) 36612734

www.mapnaturbine.com

GR684-0